Uluslararası İleri Doğa Bilimleri ve Mühendislik Araştırmaları Dergisi
Sayı 7, S. 104-114, 10, 2023
© Telif hakkı IJANSER'e aittir
Araştırma Makalesi

IJANSER
https://alls-academy.com/index.php/ijanser
ISSN: 2980-0811

International Journal of Advanced Natural Sciences and Engineering Researches
Volume 7, pp. 104-114, 10, 2023
Copyright © 2023 IJANSER
Research Article

Synthesis of Cobalt-Free, Low-Cost Layered $LiNi_{0.6}Mn_{0.2}Fe_{0.2}O_2$ (NMF622) Cathode Electrodes for Next Generation Lithium-Ion Batteries

Sümeyye KILIÇ*, Büşra OĞUZ[2] and Mehmet Oğuz GÜLER[3]

[1]*Engineering Faculty, Department of Metallurgical & Materials Engineering, Sakarya University, Turkey*
[2] *Engineering Faculty, Department of Metallurgical & Materials Engineering, Sakarya University, Turkey*
[3] *Engineering Faculty, Department of Metallurgical & Materials Engineering, Sakarya University, Turkey*

(sumeyye.kilic9@ogr.sakarya.edu.tr) Email of the corresponding author

(Received: 12 October 2023, Accepted: 23 October 2023)

(2nd International Conference on Recent Academic Studies ICRAS 2023, October 19-20, 2023)

ATIF/REFERENCE: Kılıç, S., Oğuz, B. & Güler, M. O. (2023). Synthesis of Cobalt-Free, Low-Cost Layered $LiNi_{0.6}Mn_{0.2}Fe_{0.2}O_2$ (NMF622) Cathode Electrodes for Next Generation Lithium-Ion Batteries. *International Journal of Advanced Natural Sciences and Engineering Researches*, 7(10), 104-114.

Abstract – In this research, we synthesized $LiNi_{0.6}Mn_{0.2}Fe_{0.2}O_2$ (NMF622) cathodes by substituting iron for cobalt in the cathode electrodes, which are typically associated with the chemistry of $LiNi_{0.6}Mn_{0.2}Co_{0.2}O_2$ (NMC622) cathode material used in lithium-ion batteries (LIBs). The production of NMF622 nanoparticles was achieved using the sol-gel method, incorporating metal salts as key components for structure formation. We meticulously examined the structure of NMF622 nanoparticles and electrodes through X-ray diffraction (XRD) and field emission scanning electron microscopy (FESEM), revealing the absence of impurities in the NMF622 nanopowders. Our FESEM analysis further determined particle sizes ranging from 30 to 110 nm. To evaluate the performance of NMF622 cathodes, we conducted galvanostatic charge and discharge tests at a rate of 1C within the potential range of 2.0 to 4.6 volts. Notably, the NMF622 cathodes exhibited various capacities at different rates, including 211.86, 206.07, 198.68, 191.56, 167.16, 154.99, 135.62, 115.96, 188.36, 195.36, 202.46, and 209.3 mAh/g at different C-rates. Electrochemical impedance tests indicated that all resistance values increased with the number of cycles. This study represents a significant development and evaluation of NMF cathodes, which are proposed as an alternative to NMC chemistry. As a result, it led to a substantial 60% reduction in cell manufacturing costs compared to NMC chemistry. Furthermore, the environmentally conscious choice of using iron instead of cobalt, along with the use of water-soluble binders, contributed to a reduction in toxicity.

Keywords – $LiNi_{0.6}Mn_{0.2}Fe_{0.2}O_2$ (NMF622), Layered Cathode Material, Cobalt-Free, $LiNi_{0.6}Mn_{0.2}Co_{0.2}O_2$ (NMC622), Lithium-Ion

I. INTRODUCTION

The layered $LiCoO_2$ compound, which has a high theoretical capacity (274 mAh/g) and theoretical volume capacity (1363 mAh/cm^3), was the first cathode material in Li-ion batteries to be commercially used. Another appealing aspect of this material is its high discharge voltage and good cycle performance [1]. However, this cathode material has major drawbacks. Among the commercially available cathode materials, $LiCoO_2$ has the lowest thermal stability, leading to the release of oxygen under operating conditions over a particular temperature, causing unexpected cell reactions. However, the toxicity of cobalt and its high cost have prompted a quest for alternative elements that can replace cobalt. Given its similar crystal structure, $LiNiO_2$ may be an adequate alternative to $LiCoO_2$. This cathode compound is inexpensive and has a large capacity [2-5]. However, this cathode material is not commonly used commercially. This

occurs because Ni^{+} ions block lithium diffusion pathways during the intercalation process in pure $LiNiO_2$, resulting in thermal instability and decomposition at high temperatures. Another cathode compound used in LIBs is $LiNi_{0.8}Co_{0.15}Al_{0.05}O_2$ (NCA), which has a high reversible specific capacity of 265 mAh/g compared with $LiCoO_2$.

The most important manufacturers of this cathode compound are Panasonic and Tesla. When the NCA x value in the $LiNi_xCo_yAl_zO_2$ formulation is greater than or equal to 0.8, it is considered nickel-rich. Reducing the amount of cobalt in the compound provides an advantage in terms of cost, and the amount of energy stored in the battery is also increased with an increase in nickel content. However, it should be noted that an increase in nickel content also facilitates thermal degradation [5-10]. $LiMnO_2$ cathode compounds, which are more cost-effective and less toxic than cobalt and nickel elements synthesized in the past, are widely used. However, these compounds still have several issues, such as the tendency to revert to the spinel structure during the intercalation process and the leaching of manganese ions from the layered structure as a result of electrochemical cycles. Researchers have developed a Li $(Ni_{0.5}Mn_{0.5})O_2$ cathode compound to address these issues by doping nickel ions into the $LiMnO_2$ structure. This improves the mobility of both lithium and nickel ions and has an energy density to $LiCoO_2$ [11-15]. In addition, researchers have observed that stability is further increased by adding cobalt to this compound, resulting in the formation of $LiNi_xCo_yMn_zO_2$ (NMC) which is still in commercial use today. In the cathode compound known as NMC, lithium ions are located in the 3a region, whereas nickel, manganese, and cobalt ions, which have oxygen atoms in the 3b and 6c regions, are in a mixed valency state. The cation mixture of Li^{+} (0.76 Å) and Ni^{2+} (0.69 Å) occurs because of the close proximity of their ionic radii, with nickel occupying regions typically occupied by lithium in the 3a regions [15-18]. There have been studies on the synthesis and electrochemical properties of $Li(Ni_{1/3}Mn_{1/3}Co_{1/3})O_2$ cathode electrodes, such as those conducted by Dahn and Ohzuku. Subsequently, research has focused on new synthesis methods and surface coatings that incorporate NMC species in different stoichiometric ratios, resulting in the synthesis of higher-capacity cathode materials by varying the ratios of transition metals. This type of cathode material exhibits polymorphic transformations that occur when it changes from a layered structure to a spinel structure during certain cycles. This transformation is caused by the migration of manganese atoms from tetrahedral positions in the lithium layers during intercalation and the migration of lithium atoms to octahedral positions, leaving the manganese atoms in empty positions. These atom migrations negatively affect the electrochemical properties of the structure and decrease its performance. To solve this problem, researchers have used alkali metals such as sodium, potassium, and magnesium to fill the octahedral cavities and prevent ion migration to the tetrahedral cavities. Another issue that occurs in these cathode compounds is the irreversible loss of lithium and oxidation of the electrolyte, which occurs when the Li_2MnO_3 phase is activated when the voltage exceeds 4.4 V during the first charge. This activated phase releases Li_2O into the electrolyte, preventing lithium ions from returning to the cathode and causing oxygen to react with the electrolyte, forming an oxide layer. These issues lead to capacity losses and performance drops in subsequent cycles. [19,25]. In this study, we introduced an innovative approach, which involved the replacement of cobalt with iron in cathode electrodes. Specifically, we utilized NMC622 chemistry to synthesize NMF622 cathode electrodes. This strategic substitution not only addressed the issue of toxicity associated with cobalt, a heavy metal commonly found in lithium-ion batteries but also delivered significant cost advantages. Cobalt typically constitutes a substantial portion of cell manufacturing costs, making the use of iron a more cost-effective alternative. Our primary objective was to develop cathode electrodes that not only showcased superior cyclic performance but also enhanced stability. Ultimately, our aim was to increase the commercial viability of this innovative approach, which holds promise for the future of lithium-ion battery technology.

II. Materials and Method

A. *Synthesis of $LiNi_{0.6}Mn_{0.2}Fe_{0.2}O_2$ (NMF622) nanopowders*

NMF622 nanopowders were synthesized using the sol–gel method, as shown in Figure 1. The first

step of this method, known as sol–gel, involves the formation of an inorganic polymer through condensation and hydrolysis reactions.
Initially, $C_2H_3LiO_2.2H_2O$, $Ni(CH_3COO)_2.4H_2O$, $Mn(CH_3COO)_2.4H_2O$, and $Fe(NO_3)_3.9H_2O$ were added to 80 ml of distilled water in stoichiometric ratios and mixed in a magnetic stirrer for 24 h. Afterward, NH_4OH was added to adjust the pH, and the NH_4OH was removed by heating at 80°C.
The resulting mixture forms a colloidal suspension, called a "sol," which solidifies into a "gel" as the temperature decreases [26]. After the gel was obtained, the powders were dried and heat-treated. The final NMF622 nanopowders were obtained by calcination at 100 °C for 24 hours, 350 °C for 3 hours, and 7000 °C for 6 h.

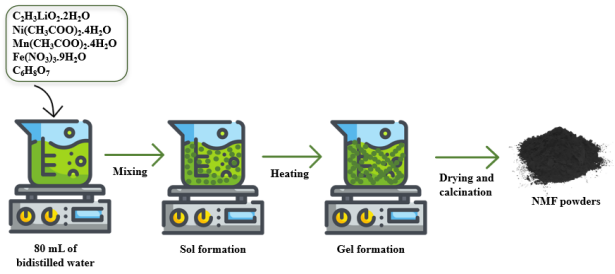

Figure 1. Synthesis of NMF622 nanopowders by sol-gel method.

B. *Synthesis of $LiNi_{0.6}Mn_{0.2}Fe_{0.2}O_2$ (NMF622) cathode electrodes and production of coin cells*

The NMF622 cathode electrodes used in this study were prepared using the conventional slurry method. The cathode slurry contained the following components: 30 mL of distilled water, 2.5% carboxymethyl cellulose (CMC), 2.5% styrene butadiene rubber (SBR), 10% Super-P, and 85% NMF622 nanopowder (Figure 2.). These components were mixed in a magnetic stirrer for 2 h. Then, it was applied to aluminum foil to a thickness of 300 µm using a doctor's blade. The resulting cathodes were dried in a vacuum oven at 85°C for 24 h. The electrodes were then cut to the appropriate size for battery pressing using an electrode-cutting device. This study performed half- and full-cell tests using CR2032 coin-type cells. Polypropylene (PP) was used as the separator, and $LiPF_6$ was used as the electrolyte.

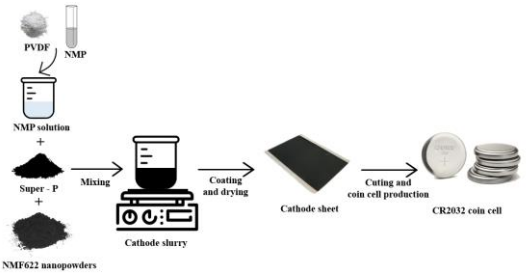

Figure 2. Electrode preparation and battery assembly processes.

C. *Metarial characterization*

The analyzed nanopowders were determined using Cu radiation in an XRD device named Rigaku DMax 2200 with a scanning speed of 2°/min between 10° and 80°. The use of FE-SEM (FEI Quanta Q400) and energy-dispersive X-ray spectroscopy (EDS) allowed the investigation of the sample's morphology and chemical composition. Using a Kaiser RXN1 instrument, Raman spectra were collected. In this study, the laser wavelength was 785 nm. The NMF622 cathodes were tested for galvanostatic charge/discharge tests between 2.0 and 4.6 V at 1C (1C = 276 mAh/g) for 500 cycles. EIS measurements were taken in the frequency range of 0.01–100 kHz to investigate the conductivity and kinetics of these materials.

RESULTS AND DISCUSSION

A. *Determination of chemical, physical, and morphological properties*

Figure 3. shows the findings of an X-ray diffraction (XRD) study of NMF622 nanopowder prepared by the sol–gel technique. The diffraction patterns were obtained as a result of the analysis. The narrow diffraction peaks of the NMF622 nanopowder can be attributed to the homogenous distribution of cations in the structure and the high crystallinity of these powders. On the other hand, it has α - $NaFeO_2$ type structure with an R-3m space group. The ratio of $I_{(003)}/I_{(104)}$ peaks is a critical indicator of the partial change in the occupancy state of Li and transition metal ions or cation mixing between sites. The reason for this is that Li^+ and Ni^{+2} ions have similar bonding structures in the R-3m structure and Li/Ni anticide defects of similar ionic diameters occur [27-29]. (006)/(102) and (108)/(110) diffraction pairs play a significant role in cathode materials with layered structures. The

obvious separation of these diffraction pairs demonstrates that the cathode materials with layered structures have a good hexagonal arrangement. It is also responsible for assisting lithium intercalation and deintercalation during the charging and discharging procedures. In cathode compounds with a layered structure such as NMF, the electrochemical properties are improved with an increase in the lattice parameter value called c.

This phenomenon can be attributed to the ability of lithium ions to traverse a wider range within the matrix [30-32]. Notably, the lattice distortion, defined by the c/a ratio of 4.983, and the cation mixture, reflected in the $I_{(003)}/I_{(104)}$ ratio of 1.428, further illuminate this behavior. It's worth mentioning that the R ratio, computed at 0.396, underscores the prevalence of the hexagonal lattice structure, indicating only minimal deviation from the cubic structure.

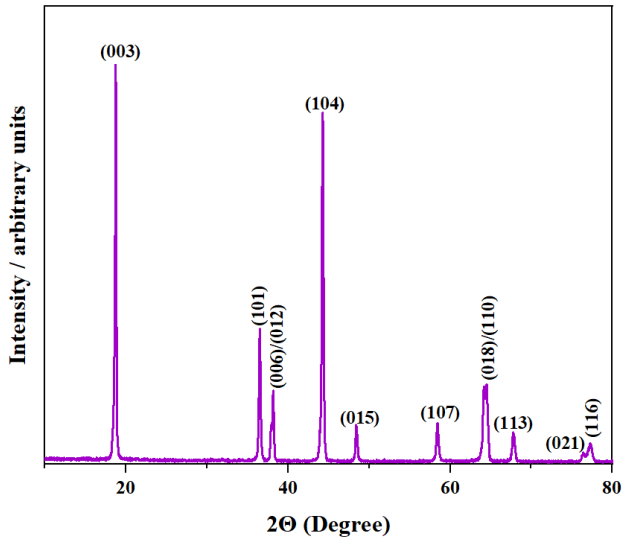

Figure 3. XRD analysis results of NMF622 nanopowder.

Table 1. Lattice parameter values of NMF622 nanopowder.

Sample	a (Å)	c (Å)	c/a	$I_{(003)}/I_{(104)}$	R
NMF622	2,853	14,217	4.983	1.428	0.396

To investigate the Raman spectroscopy of NMF622 nanopowder, we first investigated the single-component oxide structures that form this layered structure. The NMF structure can be thought of as a solid solution of $LiFeO_2$, $LiMnO_2$, and $LiNiO_2$. Polarization occurs because of the electromagnetic field applied to these solid solutions. Because of this polarization, two distinct vibration modes, A_{1g} and E_g, corresponding to the M– O stretch and the O–M–O bending in the plane, emerge. The detected vibration modes in $LiFeO_2$ are clearly visible at A_{1g}: 533 cm^{-1} and E_g: 646 cm^{-1} wavelengths. The A_{1g} vibrational mode occurs at higher wavelengths in $LiMnO_2$ [33-35].

This can be attributed to the higher polarization of electrons in the t_{2g}. In the case of $LiNiO_2$, the A_{1g} mode becomes apparent in the spectral range of 560-600 cm^{-1}, primarily due to the varying oxidation states of nickel ions. As depicted in Figure 4, two distinct vibration modes known as A_{1g} and E_g manifest at 430 cm^{-1} and 557 cm^{-1}, respectively. These modes are associated with the stretching of M–O bonds and the bending of O–M–O angles within the plane of the NMF622 nanopowder. It's important to note that the presence of Super-P in the slurry composition of the NMF622 cathode contributes to the detection of the D and G bands, prominently seen as strong peaks at 1352 cm^{-1} and 1602 cm^{-1}. The D band is categorized as a double resonance peak due to the irregularities in carbon sequencing, and its heightened intensity suggests the presence of additional sp^3 carbons. The G band exhibits impurities and irregularities stemming from the first-order scattering of the E_{2g} phonon in the sp^2 carbon-carbon bonds [35-38].

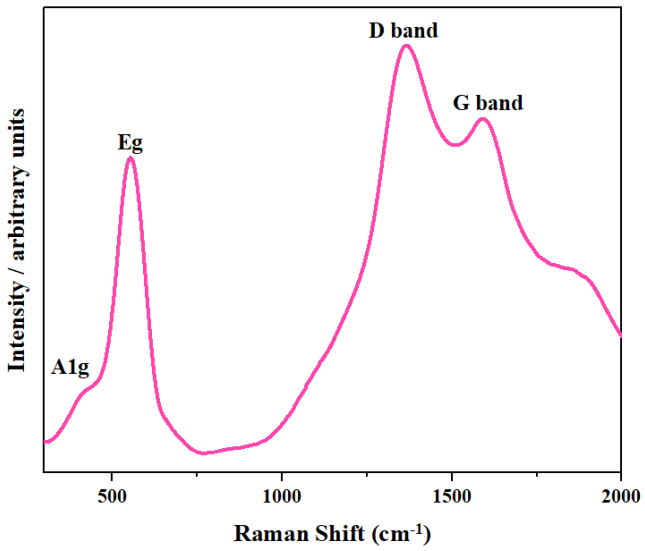

Figure 4. Raman spectroscopy of the NMF622 cathode electrode.

Figure 5. shows FESEM images and dot mapping analysis of NMF622 nanopowders synthesized using the sol–gel technique at ×50 000 and ×200 000 magnifications. All grains formed after the two-

stage calcination process have a polyhedron structure and are partially sintered with each other, with radii ranging from 30 to 110 nm. The excess of oxygen in the structure is caused by the fact that the grain structures, which represent the lighter grains in the FESEM image and are characterized as white, are oxidized, as confirmed by the EDS analysis (Figure 6.).

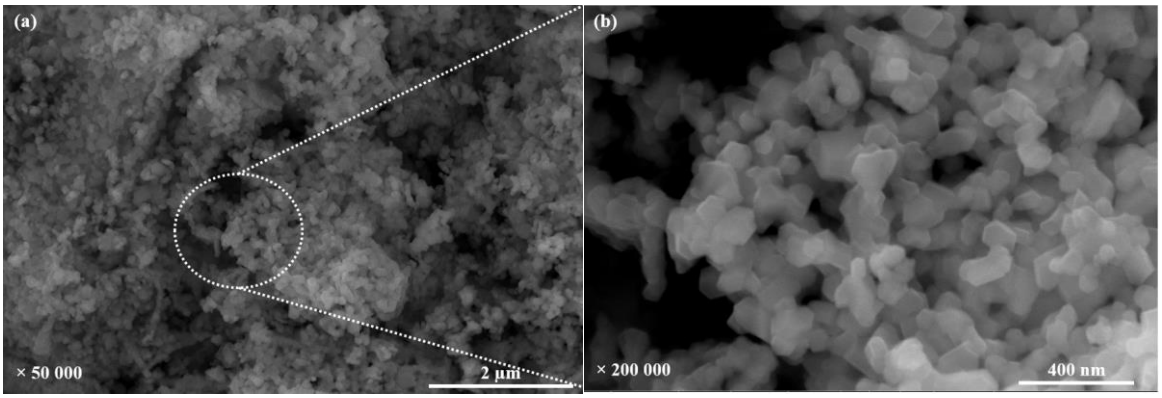

Figure 5. FESEM image of the NMF622 nanopowder. (a) ×50 000 (b) at 200 000 magnification.

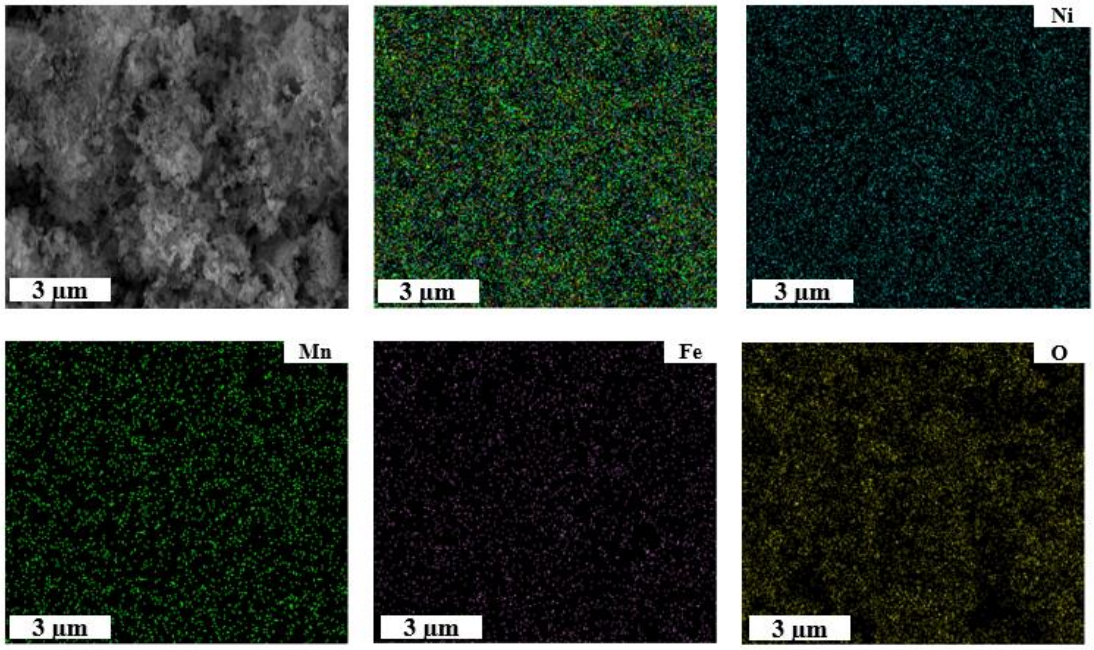

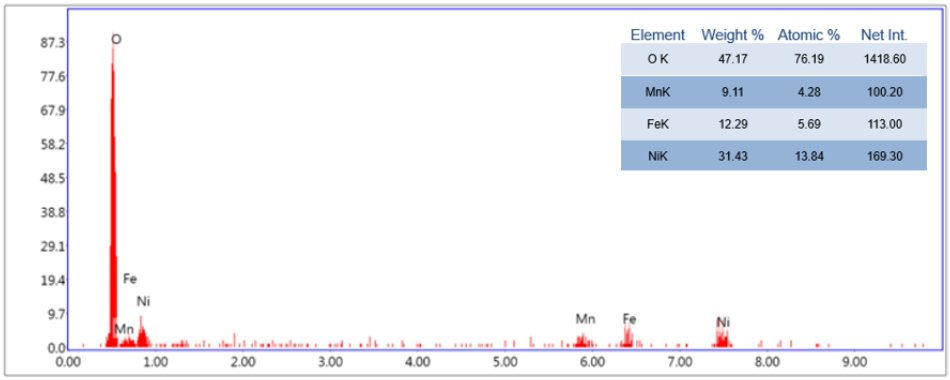

Figure 6. Dot mapping analysis and EDS pattern of NMF622 nanopowder.

B. *Electrochemical characterization*

A cyclic voltammetry test was applied to examine the phase transformations that occur in the structure of the cathode electrodes obtained from NMF nanopowders during the charging and discharging processes, and to observe the kinetic behavior of this electrode. Test conditions were carried out between 2.0 V and 4.6 V with a scanning rate of 0.1 mV/s. The data obtained because of the test are shown in Figure 7. On the CV curve of the NMF622 cathode, one can observe a peak for oxidation and one for reduction. The anodic peak is observed at 3.80 V, and the cathodic peak is observed at 3.45 V. The oxidation peak is due to the conversion of Mn^{+3} to Mn^{+4}. During discharge and at 3.45 V, the reduction peak to Mn^{+4} belongs to Mn^{+3}. At about 3.25 and 4.15 V, the absence of oxidation or reduction peaks in the structure indicates that Fe and Ni ions are still present as +2 [39,40].

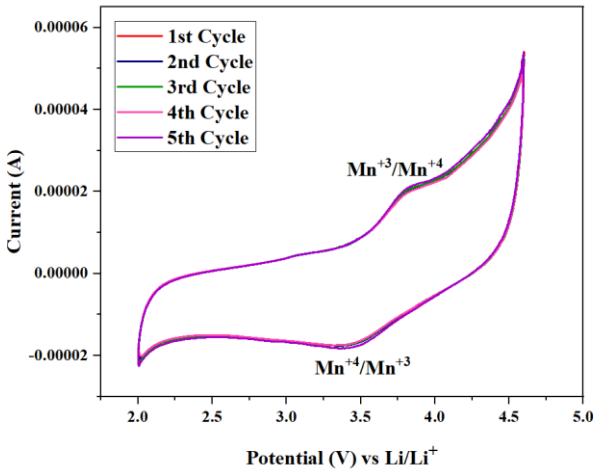

Figure 7. Cyclic voltammetry (CV) curve of the NMF622 cathode electrode.

The diffusion ability of Li^+ ions in the NMF622 sample enables us to determine the differences between the maximum voltages of the redox plateaus in the CV curve. The decrease in the differential between these plateaus indicates that diffusion happens quickly and the electrochemical process is efficient. The CV curve of the NMF622 cathode electrode reveals almost no variation in voltage levels between cycles, indicating low polarization. The NMF cathode electrode's redox potentials and polarization values are observed throughout the course of five cycles.

Figure 8. depicts the impedance spectra of NMF622 electrodes before and after the cycle (1^{st} cycle, 250^{th} cycle, and 500^{th} cycle) using a Nyquist diagram. EIS measurements were taken in the frequency range of 0.01 Hz - 100 kHz to investigate the conductivity and kinetics of these materials. Simultaneously, the equivalent circuit supplement is plotted on the graph. The graph shows that a semicircle and a linear straight line are formed. The charge transfer resistance (R_{ct}) is expressed by the semicircle's diameter, and this resistance is identical to the polarization resistance (R_p). Furthermore, the semicircle is in the high-frequency region, and the larger the diameter of this circle, the greater the resistance and the higher the concentration. The linear part is known as the low-frequency region because it includes diffusion information. This curved line also represents the Warburg impedance [41,42]. The charge transfer resistances of the electrodes are 43.23 Ω, 46.89 Ω, 121.3 Ω, and 168.6 Ω, respectively, as shown in Table 2.

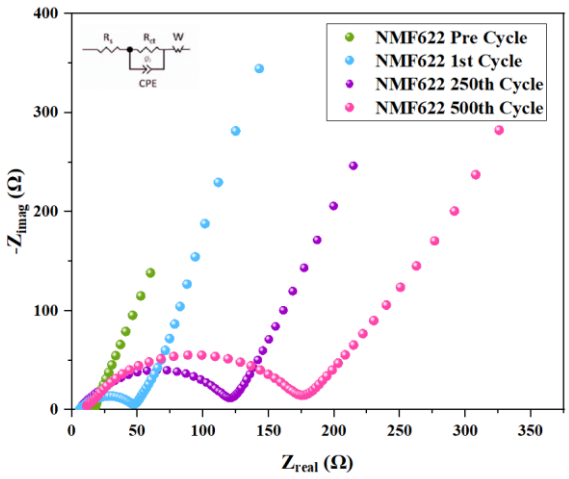

Figure 8. Impedance spectra of cathode electrodes pre and after-cycle.

The charge transfer resistance exhibits a noticeable increment with an increasing number of cycles. Notably, there were minimal alterations observed in the values of Rs. Additionally, it's evident that the sample thicknesses increase as the number of cycles progresses. This phenomenon can be attributed to both the growing number of cycles and an augmented electrostatic repulsion between the MO_6 layers. Consequently, this leads to an increase in the c/a ratio, often referred to as lattice distortion.

The increase in the c-axis dimension correlates with an expansion in the sample thickness. Before the cycling process, the NMF622 cathode electrode exhibited the lowest charge transfer resistance, primarily owing to the limited occurrence of side reactions between the active material and the electrolyte. Additionally, the smaller semicircle diameter observed for the NMF622 cathode electrode prior to cycling signifies that the fabricated electrode possesses a stable structure, facilitates rapid electrochemical reactions, and offers enhanced ionic conductivity. In stark contrast, the cathode electrode at the 500th cycle exhibited the highest charge transfer resistance. This phenomenon can be attributed to the development of a diffusion barrier for Li^+ ions, stemming from the formation of irregular layers between the plates and the consequential increase in polarization.

Table 2. Lattice parameter values of NMF622 nanopowder.

Sample	Rs (Ω)	Rct (Ω)	Thickness (mm)
NMF622 Pre Cycle	4.469	43.23	0.0266
NMF622 1st Cycle	5.757	46.89	0.0296
NMF622 250th Cycle	6.67	121.3	0.0456
NMF622 500th Cycle	9.689	168.6	0.0617

Figure 9. shows the diffusion coefficient graph of the cathode electrodes in the pre-cycle, 1. cycle, 250. cycle and 500. cycle, Table 3. displays the diffusion coefficients (Li^+) and values derived using this graph.

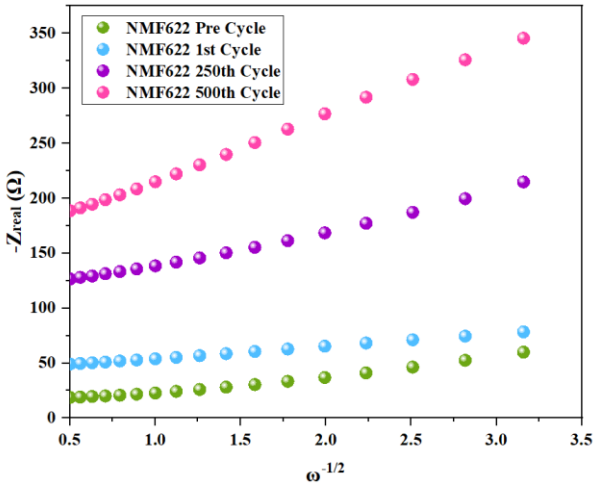

Figure 9. The relationship between -Zreal vs $\omega^{-1/2}$ graphs of NMF622 before and after cycling (1st cycle, 250th cycle and 500th cycle).

Table 3 presents the diffusion coefficients (Li^+) and their corresponding values extracted from the graph. As per the data in Table 3, prior to the cycling process, NMF622 exhibited the lowest Li^+ diffusion coefficient. This can be attributed to limited grain mobility at high frequencies, resulting in reduced diffusion. Conversely, lower frequencies facilitate greater particle diffusion, leading to higher diffusion coefficients. A high diffusion coefficient is a desirable trait in the manufactured cathode electrodes, primarily to support high load density and rapid capacity. Nevertheless, it's evident from the calculations that the diffusion of Li^+ ions in the NMF622 cathode electrode during the 500th cycle has become increasingly challenging. The hindrance of lithium-ion diffusion significantly impacts the cycling performance of the cathode electrode compounds. Pre-cycling, NMF622 boasted the highest diffusion coefficient among the

compounds, signifying superior kinetic performance and cycle life when compared to other electrodes. This underscores the enhanced kinetic performance within the cathode electrode.

Table 3. σ and D_{Li+} values of NMF622 cathode electrodes before and after cycling.

Sample	σ (ω·s$^{-1/2}$)	D_{Li}^{+} (cm^2·s^{-1})
NMF622 Pre Cycle	161.3048	$3.37892.10^{-10}$
NMF622 1st Cycle	333.6863	$7.8958.10^{-11}$
NMF622 250th Cycle	1477.938	$4.02495.10^{-12}$
NMF622 500th Cycle	2407.157	$1.51727.10^{-12}$

NMF622 cathode electrodes were tested for 500 cycles at 1C between 2.0 and 4.6 Volts (1C = 276 mAh/g). The specific capacities of the NMF622 cathode electrode at the end of the first, 250. and 500. cycles were determined to be 191.56 mAh/g, 179.21 mAh/g, and 162.48 mAh/g, respectively, as shown in Table 4. Among other layered cathode materials, the NMF622 cathode electrode shows promise with a high specific capacity of 191.56 mAh/g. According to the study's findings, doping the cathode material will improve performance and yield the desired capacity value.

By replacing the iron in the structure for cobalt, the cost of the NMC cathode material will be greatly reduced. Additionally, toxicity, one of the main issues with the element cobalt, will be prevented. The cathode electrodes' capacitance losses are shown in Table 4. The capacitance loss after 500 cycles was found to be 15.18%.

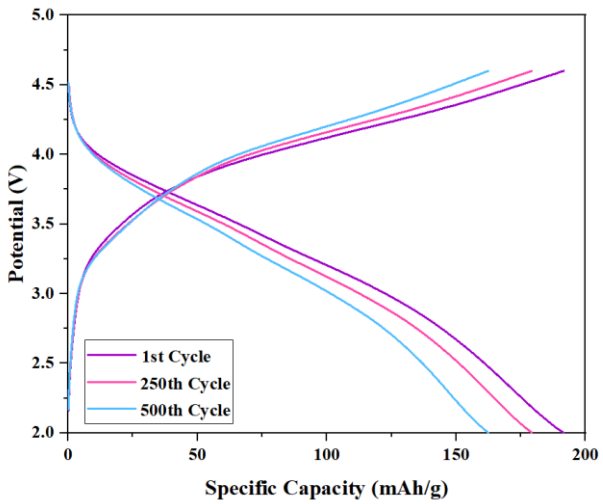

Figure 10. Galvanostatic charge/discharge curves of the cathode electrode NMF622.

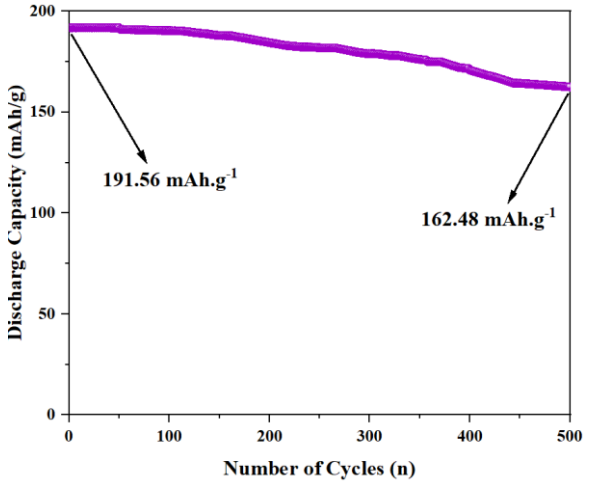

Figure 11. Graph of the specific discharge capacity of the NMF622 cathode electrode over 500 cycles.

Table 4. NMF622 cathode electrode capacity loss and galvanostatic charge/discharge results.

Sample and number of cycles	1st Cycle (mAh/g)	250th Cycle (mAh/g)	500th Cycle (mAh/g)	Capacity Loss (%)
NMF622	191.56	179.21	162.48	15.18

NMF622 cathode electrodes were tested at various C velocities and the data obtained as a result of the analysis are shown in Figure 12.' is also seen. It can be seen that the capacity value decreases with the increase in the numerical value of C. The lowest capacity value at 8C is 115 mAh/g, and the highest capacity value at C/20 speed is 211.4 mAh/g. During the first 20 cycles, no ordinary decrease in capacity values was observed. The greatest capacity loss was found during the transition from 4C to 6C speed; yet, decreasing from 8C to C/20 speed allowed the lost capacity to be regained.

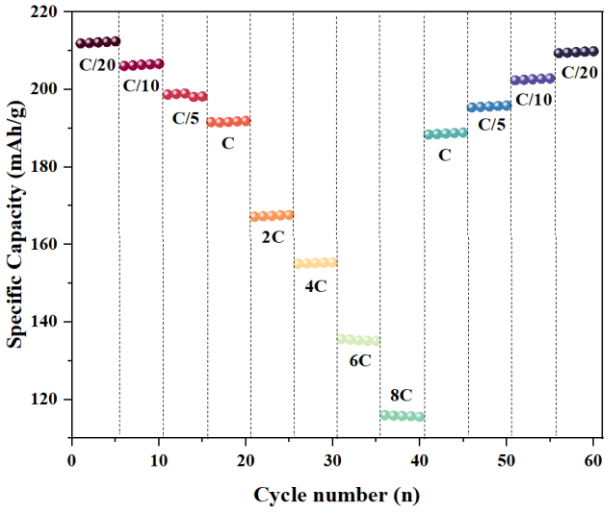

Figure 12. Number of cycles - specific capacity graph of NMF622 cathode electrodes at different charge-discharge rates.

III. RESULTS

The cost of electric vehicle batteries remains relatively high, with NMC and NCA cathode materials, known for their layered structure, remaining the most dependable choices. Meanwhile, the anode side typically utilizes graphite due to its cost-effectiveness. Efforts have been ongoing to reduce these costs, and one of the key cost-driving components is cobalt within the cathode materials. Recent experiments conducted in the past three years have yielded promising findings, particularly in the substitution of cobalt with alternative elements. Notably, manganese and iron have been successfully employed as substitutes for cobalt in NCA cathodes, although this substitution hasn't seen significant exploration in NMC cathode electrodes.

The primary goal of this research is to synthesize $LiNi_{0.6}Mn_{0.2}Fe_{0.2}O_2$ (NMF622) cathode electrodes by substituting iron for cobalt in cathode electrodes, while still utilizing $LiNi_{0.6}Mn_{0.2}Co_{0.2}O_2$ (NMC622) chemistry. The study concludes that the NMF compound demonstrates competitive potential against the proposed NMC layered material. Furthermore, the data obtained from this research affirms that using and commercializing NMF622 cathode material, as an alternative to NMC622 cathode material, leads to improved cycle performance and stability.

IV. DISCUSSION

Given the commendable cycling performance of the NMF622 cathode electrodes and the impressive retention of approximately 86% of their capacity after 500 cycles, we strongly recommend the commercialization of this cathode material. Moreover, there is promising potential for enhancing cell capacity further by incorporating various elements or carbon-based materials into the NMF622 cathode material.

V. CONCLUSION

To summarize, this study focused on the synthesis of $LiNi_{0.6}Mn_{0.2}Fe_{0.2}O_2$ (NMF622) cathode electrodes, offering insights into the development of low-cost, next-generation lithium-ion batteries with a cobalt-free layered structure. The active material used in crafting NMF622 cathode electrodes was produced through the sol-gel method. Numerous factors influence the preparation of these cathode electrodes, including the microstructural properties of the active material. Given the nanoscale nature of the active material, it demonstrated enhanced electrochemical properties. X-ray diffraction analysis confirmed the absence of impurities in the produced nanopowders, and the structure was found to be in alignment with α-$NaFeO_2$. The prepared cathode electrodes underwent 500 cycles at a 1C rate, and the results indicated that approximately 85% of the initial capacity was retained at the end of this extensive testing. This exceptional cycle performance and stability were achieved, providing a promising outlook for NMF cathode material.

In contrast to the limited attention NMF cathode material has received in prior literature, this study contributes valuable insights. It not only supports the potential of NMF material in influencing future research but also highlights the development of a competitive cathode material capable of challenging NMC chemistry.

ACKNOWLEDGMENT

The authors would like to thank the Research Development Application and Research Center (SARGEM) of Sakarya University for the study.

REFERENCES

[1] A. D. Pasquier, I. Plitz, S. Menocal, G. Amatucci, 'A Comparative Study of Li-ion Battery, Supercapacitor and Nonaqueous Asymmetric Hybrid Devices for Automotive Applications', Journal of Power Sources 115 (2003) 171–178.

[2] T. Ohzuku, R. J. Brodd, An overview of positive-electrode materials for advanced lithium-ion batteries, J. Power Sources 174 (2) (2007) 449–456.

[3] Z. Chang, Z. Chen, H. Tang, X. Z. Yuan, H. Wang, 2010. Synthesis and characterization of lamellar $LiCoO_2$ as cathode materials for lithium-ion batteries. J. N. Mater. Electrochem. Syst. 13, 107–111.

[4] R. Alcantara, G. F. Ortiz, J. L. Tirado, R. Stoyanova, E. Zhecheva, S. Ivanova, Fe^{3+} and Ni^{3+} impurity distribution and electrochemical performance of $LiCoO_2$ electrode materials for lithium ion batteries, J. Power Sources 194 (2009) 494–501.

[5] Y.C. Gonz´alez, L. Alcaraz, F.J. Alguacil, L. Barbosa, J. Gonz´alez, F.A.A. Lopez, ´ Study of the carbochlorination process with $CaCl_2$ and water leaching for the extraction of Li, Co, and Ni from spent lithium-ion batteries, Batteries (2023).

[6] Q. Yang, J. Huang, Y. Li, Y. Wang, J. Qiu, J. Zhang, H. Yu, X. Yu, H. Li, L. Chen, Surface-protected $LiCoO_2$ with ultrathin solid oxide electrolyte film for high voltage lithium ion batteries and lithium polymer batteries, J. Power Sources 388 (2018) 65–70.

[7] J. Dul, B. Vis, G. Goertz, 2021. Necessary Condition Analysis (NCA) does exactly what it should do when applied properly: a reply to a comment on NCA. Socio. Methods Res. 50 (2), 926–936.

[8] S. Hildebrand, C. Vollmer, M. Winter, F.M. Schappacher, Al_2O_3, SiO_2 and TiO_2 as Coatings for Safer $LiNi_{0.8}Co_{0.15}Al_{0.05}O_2$ Cathodes: Electrochemical Performance and Thermal Analysis by Accelerating Rate Calorimetry, J. Electrochem. Soc. 164 (9) (2017) A2190–A2198.

[9] J.B. Goodenough, K. S. Park, J. Am. Chem. Soc. 135 (4) (2013) 1167–1176.

[10] X. Zhu, Z. Wang, Y. Wang, H. Wang, C. Wang, L. Tong, M. Yi, Overcharge investigation of large format lithium-ion pouch cells with $Li(Ni_{0.6}Co_{0.2}Mn_{0.2})O_2$ cathode for electric vehicles: thermal runaway features and safety management method. Energy 2019;169:868–80.

[11] M. Chen, Z. Pan, X. Jin, Z. Chen, Y. Zhong, X. Wang, Y. Qiu, M. Xu, W. Li, Y. Zhang, Highly integrated all-manganese battery with supported oxide nanoparticles on cathode and anode by super-aligned carbon nanotubes, J. Mater. Chem. (2019).

[12] C. Shen, H. Xu, L. Liu, H. Hu, S. Chen, L. Su, L. Wang, EDTA-2 Na assisted dynamic hydrothermal synthesis of orthorhombic $LiMnO_2$ for lithium-ion battery, J. Alloys Compd. 830 (2020) 154599.

[13] Q. Liu, Y. Li, Z. Hu, D. Mao, C. Chang, F. Huang, One-step hydrothermal routine for pure-phased orthorhombic $LiMnO_2$ for Li-ion battery application, Electrochim. Acta 53 (2008) 7298-7302.

[14] S. H. Liu, X. F. Qian, J. Yin, X. D. Ma, J. Y. Yuan and Z. K. Zhu, J. Phys. Chem. Solids, 64(2003)455. S. Zhang, C. Zhu, J. K. O. Sin, and P. K. T. Mok, "A novel ultrathin elevated channel low-temperature poly-Si TFT," *IEEE Electron Device Lett.*, vol. 20, pp. 569–571, Nov. 1999.

[15] K. Ariyoshi, H. Yamamoto, Y. Yamada, Relationship between changes in ionic radius and lattice dimension of lithium manganese oxide spinels during lithium insertion/extraction, Solid State Ionics 343 (2019) 115077.

[16] H. J. Noh, S. Youn, C. S. Yoon, Y. K. Sun, Comparison of the structural and electrochemical properties of layered $Li[Ni_xCo_yMn_z]O_2$ (x = 1/3, 0.5, 0.6, 0.7, 0.8, 0.85) cathode material for lithium-ion batteries, J. Power Sources 233 (2013) 121–130.

[17] J. Wang, J. Purewal, P. Liu, J. H. Garner, S. Soukazian, E. Sherman, A. Sorenson, L. Vu, H. Tataria, M. V. Verbugge, Degradation of lithium ion batteries employing graphite negatives and nickel–cobalt–manganese oxide + spinel manganese oxide positives: Part 1, aging mechanisms and life estimation, J. Power Sources 269 (2014) 937–948.

[18] X. Fu, X. A. Zhou, D. Zhao, Y. Liang, P. Wang, N. Zhang, K. Tuo, H. Lu, X. Cai, L. Mao, S. Li, Study on electrochemical performance of Al-substitution for different cations in Li-rich Mn-based materials, Electrochim. Acta 394 (2021), 139136.

[19] L. Zhou, J. Liu, L. Huang, N. Jiang, Q. Zheng, D. Lin, Sn-doped $Li_{1.2}Mn_{0.54}Ni0.13Co_{0.13}O_2$ cathode materials for lithium-ion batteries with enhanced electrochemical performance, J. Solid State Electrochem. 21 (12) (2017) 3467–3477.

[20] A. Hammou, R. Petrone, D. Diallo, H. Gualous, Experimental analysis of the effects of discharge current-rates on the parameters of the electrical equivalent circuit for NMC and LCO Li-ion batteries, in: IECON 2022 – 48th Annual Conference of the IEEE Industrial Electronics Society, 2022, pp. 1–6.

[21] M.A. Rajaeifar, P. Ghadimi, M. Raugei, Y. Wu, O. Heidrich, Challenges and recent developments in supply and value chains of electric vehicle batteries: a sustainability perspective, Resour. Conserv. Recycl. 180 (2022), 106144.

[22] S. Wang, C. Wang, F. Lai, F. Yan, Z. Zhang, Reduction-ammoniacal leaching to recycle lithium, cobalt, and nickel from spent lithium-ion batteries with a hydrothermal method: effect of reductants and ammonium salts, Waste Manag. vol. 102 (2020) 122–130.

[23] S. Windisch-Kern, A. Holzer, L. Wiszniewski, H. Raupenstrauch, 2021. Investigation of potential recovery rates of nickel, manganese, cobalt, and particularly lithium from NMC-type cathode materials ($LiNi_xMn_yCo_zO_2$) by carbo-thermal reduction in an inductively heated carbon bed reactor. Metals 11 (11), 1844.

[24] D. Cao, Q. Li, X. Sun, Y. Wang, X. Zhao, E. Cakmak, W. Liang, A. Anderson, S. Ozcan, H. Zhu, Amphipathic binder integrating ultrathin and highly ionconductive sulfide membrane for cell-level high-energy-density all-solid-state batteries, Adv. Mater. 33 (52) (2021), 2105505.

[25] K. M€ arker, P.J. Reeves, X. Chao, K.J. Griffith, C.P. Grey, Evolution of structure and lithium dynamics in $LiNi_{0.8}Mn_{0.1}Co_{0.1}O_2$ (NMC811) cathodes during electrochemical cycling, Chem. Mater. 31 (2019) 2545e2554.

[26] N. Manousi, V. Alampanos, I. Priovolos, A. Kabir, K.G. Furton, E. Rosenberg, G. A. Zachariadis, V.F. Samanidou, Exploring sol–gel zwitterionic fabric phase sorptive extraction sorbent as a new multi-mode platform for the extraction and preconcentration of triazine herbicides from juice samples, Food Chem. 373 (2022) 131517.

[27] G. Qian, J. Zhang, S.-Q. Chu, J. Li, K. Zhang, Q. Yuan, Z.-F. Ma, P. Pianetta, L. Li, K. Jung, Y. Liu, Understanding the Mesoscale Degradation in Nickel-Rich Cathode Materials through Machine-Learning-Revealed Strain-Redox Decoupling, ACS Energy Lett. 6 (2) (2021) 687–693.

[28] J. Sicklinger, M. Metzger, H. Beyer, D. Pritzl, H.A. Gasteiger, Ambient Storage Derived Surface Contamination of NCM811 and NCM111: Performance Implications and Mitigation Strategies, J. Electrochem. Soc. 166 (2019) A2322–A2335.

[29] J. Lim, T. Hwang, D. Kim, M. Park, K. Cho, M. Cho, Intrinsic origins of crack generation in Ni-rich $LiNi_{0.8}Co_{0.1}Mn_{0.1}O_2$ layered oxide cathode material, Sci. Rep.- UK 7 (2017) 39669.

[30] Molenda, M., Dziembaj, R., Podstawka, E., Proniewicz, L. M. (2005). Changes in local structure of lithium manganese spinels (Li:Mn = 1:2) characterised by XRD, DSC, TGA, IR, and Raman spectroscopy. Journal of Physics and Chemistry of Solids, 66, 1761-1768.

[31] Gao, T., Fjellvag, H., Norby, P., A comparison study on Raman scattering properties of a and b-MnO_2. Analytica Chimica Acta, 648, 235–239, 2009.

[32] Ferrari, A.C., Raman spectroscopy of graphene and graphite: Disorder, electron–phonon coupling, doping and nonadiabatic effects, Solid State Commun., 143(1–2), 47-57. 2007.

[33] Molenda, M., Dziembaj, R., Podstawka, E., Proniewicz, L. M. (2005). Changes in local structure of lithium manganese spinels (Li:Mn = 1:2) characterised by XRD, DSC, TGA, IR, and Raman spectroscopy. Journal of Physics and Chemistry of Solids, 66, 1761-1768.

[34] Gao, T., Fjellvag, H., Norby, P., A comparison study on Raman scattering properties of a and b-MnO_2. Analytica Chimica Acta, 648, 235–239, 2009.

[35] Ferrari, A.C., Raman spectroscopy of graphene and graphite: Disorder, electron–phonon coupling, doping and nonadiabatic effects, Solid State Commun., 143(1–2), 47-57. 2007.

[36] Tuinstra, F., Koenig, J.-L., Raman spectrum of graphite, J. Chem. Phys., 53, 1126–1130, 1970.

[37] Malard, L.-M., Pimenta, M.-A., Dresselhaus, G., Dresselhaus, M.-S., C, Phys. Rep., 473, 51-87, 2009.

[38] Gupta, A., Chen, G., Joshi, P., Tadigadapa, S. Eklund, P.C., Raman scattering from high-frequency phonons in supported n-graphene layer films, Nano Lett., 6, 2667–2673, 2006.

[39] K. Shaju, G. S. Rao, and B. Chowdari, Electrochimica Acta, 48(2), 145 (2002).

[40] H. Cao, Y. Zhang, J. Zhang, B. Xia, 'Synthesis and electrochemical characteristics of layered $LiNi_{0.6}Co_{0.2}Mn_{0.2}O_2$ cathode material for lithium ion batteries', Solid State Ion. 2005, 176, 1207–1211.

[41] J. M. Zheng, Z. R. Zhang, X. B. Wu, Z. X. Dong, Z. Zhu, Y. Yang, 'The Effects of AlF_3 Coating on the Performance of $Li[Li_{0.2}Mn_{0.54}Ni_{0.13}Co_{0.13}]O_2$ Positive Electrode Material for Lithium-Ion Battery'. *J. Electrochem. Soc.* 2008, *155*, A775–A782.

[42] X. He, C. Y. Du, B. Shen, C. Chen, X. Xu, Y. Wang, P. Zuo, Y. Ma, X. Cheng, G. Yin, 'Electronically conductive Sb-doped SnO_2 nanoparticles coated $LiNi_{0.8}Co_{0.15}Al_{0.05}O_2$ cathode material with enhanced electrochemical properties for Li-ion batteries', Electrochimica Acta. 2017, 236:273-279.